# Astronomy Lab

## K) Basics of Infrared Observation

**Supervisor: Markus Mugrauer**
**Last Update: April 2026**

# 1 Introduction

In 1800, the Hannover-born astronomer William Herschel (1738 - 1822), who had become famous for discovering the planet Uranus, discovered an invisible component of the solar spectrum, which he was able to detect at its long-wave red end. This infrared radiation could be detected by thermometers placed inside and outside the solar spectrum (see Fig. 1). Today, the infrared spectral range is generally divided into three parts: near (0.75 - 5 $\mu$m), mid (5 - 25 $\mu$m), and far (25 - 350 $\mu$m) infrared.

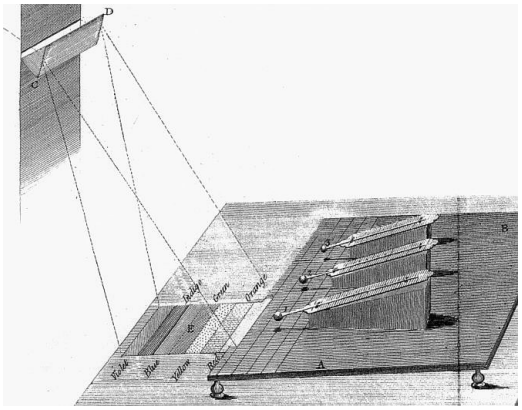

Figure 1: The setup shown here made it possible to detect infrared radiation by measuring temperature for the first time.

Observations of the night sky in infrared have led to many interesting astronomical discoveries in recent years. These include direct observations of the first low-mass substellar objects (brown dwarfs or planets), investigations of star-forming regions, exploration of the center of the Milky Way, and the detection of distant and therefore strongly redshifted galaxies.

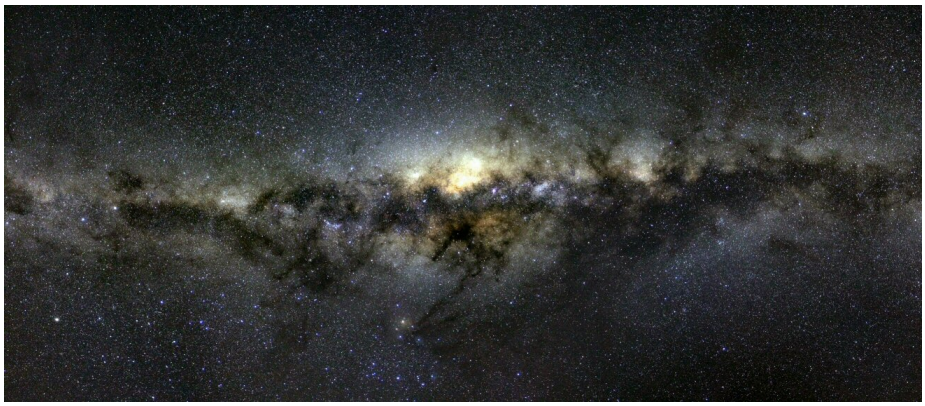

Figure 2: The central region of our galaxy, the Milky Way, photographed in the visible spectrum. Dense clouds of gas and dust obscure the view of the galaxy's center. The yellowish star Antares can be seen in the lower center of the image. Photo: M. Mugrauer

When observing our Milky Way in the visible part of the electromagnetic spectrum, many dark bands and filaments along the galactic plane are noticeable (see Fig. 2). These dark regions consist of dust and gas masses that are located in front of the stars of our Milky Way and absorb and scatter their light. The absorption and scattering of electromagnetic radiation, or its extinction $A_\lambda$ for short, depends on the wavelength:

$$A_\lambda \propto \lambda^{-1.75}$$

**Question:** Determine the extinction ratio between visible light (0.6 $\mu$m) and infrared radiation at 2 $\mu$m and 10 $\mu$m, respectively.

Star-forming regions are deeply embedded in clouds of gas and dust and are therefore difficult or impossible to observe in visible light, as the light from the newly forming stars is (almost) completely absorbed. In the near infrared, however, the stars are visible because infrared radiation can penetrate the gas and dust masses.

Known star-forming regions can be seen in Fig. 2. They are located north of Antares in the constellation Scorpius and extend into the constellation Ophiuchus. South of Antares, another star-forming region can be found in the constellation Lupus.

The birthplaces of stars can be described simply as large clouds of dust and gas. If the internal gas pressure of the clouds is lower than the gravitational pressure generated by gravity, the clouds collapse under their own gravity. In general, a cloud is only gravitationally stable if its mass does not exceed the so-called Jeans mass $M_{\text{Jeans}}$. The Jeans mass can be calculated using the Boltzmann constant $k$, the gravitational constant $G$, the mean particle mass $\mu$, and the density of the cloud $\rho$, and the following applies:

$$M_{\text{Jeans}} = 5.46(\tfrac{kT}{G\mu})^{1.5}\rho^{-0.5}$$

More massive clouds are gravitationally unstable and collapse in what is known as the free-fall time:

$$\tau_{\text{ff}} = \sqrt{\tfrac{3\pi}{32G\rho}}$$

For the interstellar medium with $T = 10\,\text{K}$ and a density of $1\,\text{H-atom/cm}^3$, this results in a Jeans mass of $M_{\text{Jeans}} \approx 3000\,M_\odot$. As this estimate shows, the clouds must have comparatively large masses in order for stars to form in them at all. When the clouds collapse, only the average density increases at first (same mass with smaller volume). The temperature remains approximately constant because the gravitational energy released during contraction can be radiated outward. However, the increase in density reduces the Jeans mass, and so gradually, increasingly less massive parts of the cloud become gravitationally unstable. A large cloud thus gradually breaks down into smaller and smaller fragments that are also gravitationally unstable (fragmentation).

**Question:** Determine the minimum density (in kg/m$^3$ and in atoms/cm$^3$) of a gas cloud ($M = 1\,M_\odot$, $T = 10\,\mathrm{K}$) for it to collapse under its own gravity. How long (in years) does it take for this gas cloud to collapse? To do this, calculate the free-fall time $\tau_{\mathrm{ff}}$.

These individual fragments give rise to either stars with masses greater than $0.078\,M_\odot$ or the less massive brown dwarfs ($0.013\,M_\odot < m < 0.078\,M_\odot$). As the large gas cloud continues to contract, the gas density increases and the gas eventually becomes opaque to radiation. Since both the density and temperature of the cloud are now rising sharply, the Jeans mass does not decrease further, but reaches a minimum at approximately $0.013\,M_\odot$.

Many of the newly formed stars are surrounded by disks. The accretion of disk material and the gravitational instability of the disks lead to the formation of planets orbiting their parent stars. Since the lifetime of the disks is only a few million years, planet formation must also take place within this period. The mass of a planet ($m < 0.013\,M_\odot$) is so small that the pressure and temperature in its core are insufficient to initiate nuclear fusion processes. The planet's only energy supply is the gravitational energy released during its collapse, which the planet then radiates over time. In just a few million years, the planets cool down rapidly and become increasingly dim.

Brown dwarfs already have such a high mass ($0.013\,M_\odot < m < 0.078\,M_\odot$) that deuterium burning can ignite in their cores. Convection causes the gas inside the brown dwarf to mix continuously. Cool gas from the surface sinks toward the core, and hot gas rises from the core to the surface. Due to this mixing of the atmosphere, all of the deuterium eventually reaches the core, where it is fused. After several million years, all the deuterium is consumed and the internal energy source is exhausted. From this point on, brown dwarfs cool down and become increasingly dim. Brown dwarfs and planets are also referred to as substellar objects because they cannot ignite long-lasting nuclear fusion processes in their interiors.

The stellar objects are the stars. The temperatures and pressures at the center of a star are so high that hydrogen can fuse into helium (hydrogen burning). This provides the star with a stable source of energy that will continue to supply energy until the entire supply of hydrogen in the core has been used up. In sun-like stars, the hydrogen in the core lasts for many billions of years. During this period, known as the main sequence phase, the temperature and luminosity of the star change only very slowly.

If a brown dwarf or planet orbits a star as a companion, the brightness ratio between the two objects depends heavily on the age of the system. Since substellar objects become increasingly dim over time, they are easier to detect directly in young systems than in older ones. The difference in brightness between the hot star and the cool substellar companion depends on the wavelength and reaches a minimum in the near infrared.

**Question:** Calculate the brightness difference $\Delta m$ (in magnitudes) between a young hot planet ($T = 1000\,\mathrm{K}$, $R = 0.1 R_\odot$) and a sun-like star ($T = 5800\,\mathrm{K}$, $R = 1\,R_\odot$) in the visible wavelength range $\lambda = 0.55\,\mu\mathrm{m}$ and in the near infrared at $\lambda = 2\,\mu\mathrm{m}$. For simplicity, assume that both objects are black bodies[1,2].

## 1.1 Detectors

For a long time, astronomical observations could only be carried out in the visible part of the electromagnetic spectrum. Initially, observations were made with the naked eye, but in the mid-19th century, photography was successfully used as an astronomical observation technique for the first time. This made it possible to integrate the light collected by the telescope over a longer period of time, which enabled the study of faint objects (imaging and spectroscopy). The blackening of the film material is a measure of the number of photons detected.

Until the mid-1970s, film and photographic plates were the most widely used detectors in astronomy, before they were replaced by the much more light-sensitive CCD (charge-coupled device) detectors. While only one in every hundred photons darkens the emulsion in a photographic film, modern CCD detectors can detect over 90% of the photons that reach the detector. A CCD detector is made up of many individual image elements (pixels). The size of these image elements ranges between 5 and 30 $\mu$m. In the simplest case, each pixel consists of a p-doped silicon layer connected to a metal contact via a thin $SiO_2$ layer (MOS: Metal Oxide Semiconductor) to which an electrical potential is applied. When a photon strikes the semiconductor, the photoelectric effect creates an electron-hole pair, which is separated by the applied electric field before it can recombine. The charge generated is directly proportional to the number of incident photons. After exposure, the potential at the individual pixels is changed, transporting the collected charge carriers to the readout electronics. There, the charge of each pixel is determined sequentially via the voltage drop across a capacitor. The spectral sensitivity of CCD detectors based on silicon[3] ranges from approximately 0.2 $\mu$m to the near infrared.

**Question:** Determine the cutoff wavelength of a CCD detector.

Infrared detectors, which are comparable to CCD detectors in terms of pixel count and size, were first used successfully in astronomy in the mid-1980s. Unlike CCDs, the charge of each pixel in an infrared detector can be measured directly and does not first have to be transported across the entire detector. As in CCDs, the incident photons are detected by the photoelectric effect. However, due to the lower energy of infrared photons, semiconductors with correspondingly smaller band gaps must be used. The semiconductors $Hg_{0.55}Cd_{0.45}Te$ (0.5 eV) and InSb (0.23 eV) are most commonly used nowadays in infrared detectors.

[1] Spectral flux density of a black body: $F_\lambda(\lambda) = \frac{2\pi hc^2}{\lambda^5(e^{hc/kT\lambda}-1)}$

[2] Apparent brightness of an object: $m = -2.5log(F) + m_0$

[3] Energy gap of $Si$: $E_{\mathrm{gap}} = 1.12\,\mathrm{eV}$

The individual pixels of an infrared detector have a two-layer structure. The upper layer consists of a photodiode that is sensitive to infrared radiation. The layer below contains a silicon field-effect transistor, which is used to measure the diode voltage. At the beginning of each exposure, a reverse voltage is applied to the photodiode. The charge displaced in this process depends on the applied reverse voltage $U_{\text{rev}}$ and the effective diode capacitance $C$ and is simply calculated as $Q = C \cdot U_{\text{rev}}$. When photons strike the photodiode, electron-hole pairs are formed by the photoelectric effect. These pairs are separated by the internal electric field at the pn junction of the photodiode before recombination occurs. The voltage drop $\Delta U_{\text{rev}} = \Delta Q/C$ across the diode gives the amount of charge generated during the exposure time, which is directly proportional to the number of photons incident. The sensitivity of the individual pixels varies slightly. However, this effect can be corrected by capturing an evenly illuminated area, known as a flatfield image

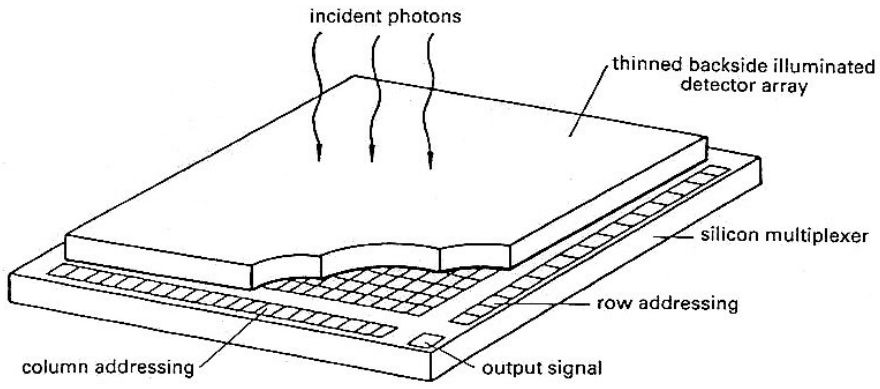


Figure 3: Structure of an infrared detector.

In addition to the charge carriers generated by the photoelectric effect in the semiconductor, the thermal energy of some electrons is also sufficient to generate electron-hole pairs in the semiconductor. To keep this so-called dark current as low as possible, infrared detectors must always be operated in a cooled state.

**Question:** Estimate the average thermal energy (in eV) of an electron in the semiconductor at $T = 300\,\text{K}$ and explain why dark current still occurs. Which infrared detector (InSb or HgCdTe) would you expect to have a higher dark current if both are at the same temperature?

## 1.2 The signal-to-noise ratio

According to Poisson statistics, the number of photons detected from a source fluctuates around the mean value $S$. This mean value corresponds to the detected signal from the source and can be calculated from the radiation flux $s$ of the source and the exposure time $t$:

$S = s \cdot t$

The standard deviation from the mean value $S$ is referred to as the photon noise $N$ of the source. According to Poisson statistics:

$$N = \sqrt{s \cdot t}$$

If the radiation flux $s$ of the source and the radiation flux of the sky background $b$ strike a pixel during the exposure time $t$, this results in a signal-to-noise ratio:

$$SNR = S/N = \frac{s \cdot t}{\sqrt{s \cdot t + b \cdot t + R^2}}$$

where $R$ is the readout noise of the detector, which in infrared detectors is caused by slight fluctuations in the reverse voltage applied to the pixels.

As long as the observed object is the brightest source, the photon noise of the source limits the $SNR$ of the image. If, on the other hand, the sky background is much brighter than the observed object, the photon noise of the background limits the $SNR$ of the image. In both cases, the $SNR$ of the image increases with the square root of the exposure time. However, this only applies to sufficiently long exposure times. With an exposure time shorter than

$$\tau_{\mathrm{RN}} \approx R^2/b$$

the photon noise of the background is smaller than the readout noise of the detector. In this range, the $SNR$ increases linearly with the exposure time (see Fig. 4).

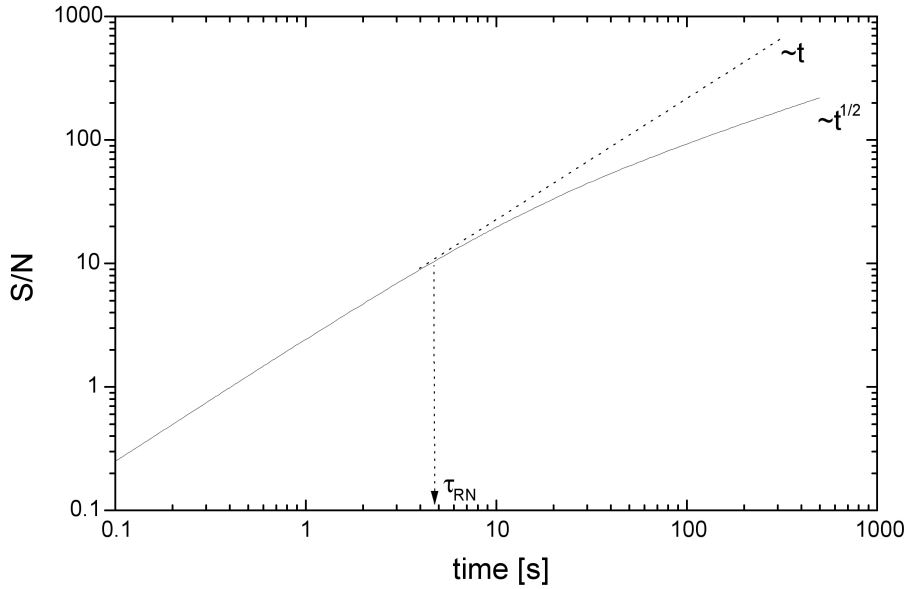


Figure 4: The dependence of the signal-to-noise ratio on the exposure time.

If $N$ images are added together, the S/N ratio of the sum of all images is $\sqrt{N}$ times higher than the $SNR$ of a single image. If the individual images are limited only by photon noise, the sum of these images has the same $SNR$ as a single image with a correspondingly longer exposure time.

If, on the other hand, the readout noise of the detector dominates the individual images, the $SNR$ of the sum of these images is smaller than the $SNR$ of a single image with a correspondingly longer exposure time.

When observing in the near infrared (1 - 2.5 $\mu$m), $\tau_{\mathrm{RN}}$ is wavelength-dependent and ranges from a few seconds to a few minutes. At even longer wavelengths, $\tau_{\mathrm{RN}}$ shortens significantly to less than a second due to the ever-increasing background brightness.

## 1.3 Atmospheric Emission and Absorption

The Earth's atmosphere consists of a multitude of molecules. Since molecules have vibration and rotation energy states in addition to the individual energy levels of the electrostatic potential, there are significantly more energy levels available compared to a single atom. When a molecule transitions from a higher to a lower energy state, electromagnetic radiation is emitted. In the near infrared, this glow of the atmosphere (see Fig. 5) is mainly caused by the hydroxyl ion (OH), which is formed in the upper atmosphere at an altitude of approx. 90 km by the reaction:

$$H + O_3 \longrightarrow OH^{\star} + O_2$$

The ion is in a highly excited energy state and releases its energy by emitting infrared radiation. The emission of the night sky is not constant, but fluctuates irregularly by up to 10% within 15 minutes. Within one night, the brightness of the sky as a whole can vary by up to 50% Above a wavelength of 3.5 $\mu$m, the thermal radiation of the Earth's atmosphere becomes a noticeable source of interference in addition to the radiation from OH molecules.

**Question:** Determine the wavelength at which a blackbody with a temperature of $T = 30\,^{\circ}\mathrm{C}$ has the highest spectral flux density.

In the near infrared, the sky background is much brighter than in the optical spectral range and already brighter than most observable objects (see Tab. 1). This background is variable and changes its brightness within just a few minutes. In order to be able to detect faint objects, the sky background must be subtracted during observation.

For this reason, the jitter technique is used for observations in the near infrared. This involves taking many images of the object and shifting the telescope by a small angle between exposures so that all objects always fall on slightly different positions on the detector. Subtracting these individual images from each other removes the sky background from the images. The jitter technique is a very effective observation method, as the object images are used simultaneously to measure the sky background. However, for this to work, it must be ensured that

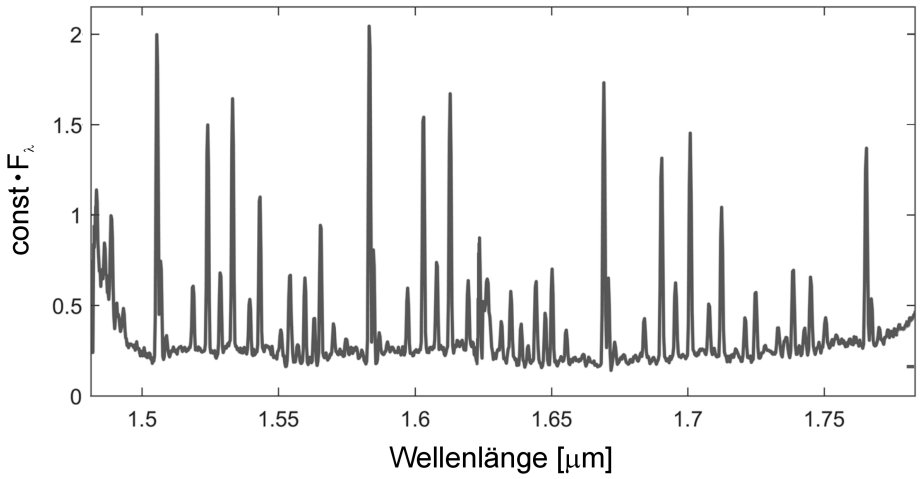


Figure 5: The emission of the Earth's atmosphere in the H-band (1.65 $\mu$m). The individual emission lines are produced by excited OH molecules in the Earth's atmosphere.

| Days since New Moon | V (0.60 $\mu$m) | J (1.25 $\mu$m) | H (1.65 $\mu$m) | K (2.16 $\mu$m) |
|---|---|---|---|---|
| 0 | 21.4 | 15.7 | 14.0 | 12.5 |
| 7 | 21.0 | 15.7 | 14.0 | 12.5 |
| 14 | 19.2 | 15.7 | 14.0 | 12.5 |

Table 1: Surface brightness [mag/arcsec$^2$] of the night sky in different bands. The brightness of the night sky depends on the phase of the moon only in the visible spectral range.

most of the detector's pixels actually only measure the sky background. When observing dense star fields or extended objects, the background must be determined using an additional image (extended jitter technique). After exposing the object, the telescope is moved to the closest possible position in the sky, where the background image can then be taken. The telescope is then moved back to the object. Subtracting the corresponding background image from each object image removes the sky background. In addition to the emission lines of OH molecules, other molecules (especially $H_2O$ and $CO_2$) produce strong absorption bands in the near infrared. Between 1.1 and 2.5 $\mu$m, the Earth's atmosphere is only transparent to electromagnetic radiation in three bands (see Fig. 6). The J-band has a central wavelength of 1.25 $\mu$m, followed by the H-band at 1.65 $\mu$m and the K-band at 2.16 $\mu$m. Special bandpass filters (J, H, K) allow observation in these wavelength ranges, which are only a few hundred nm wide.

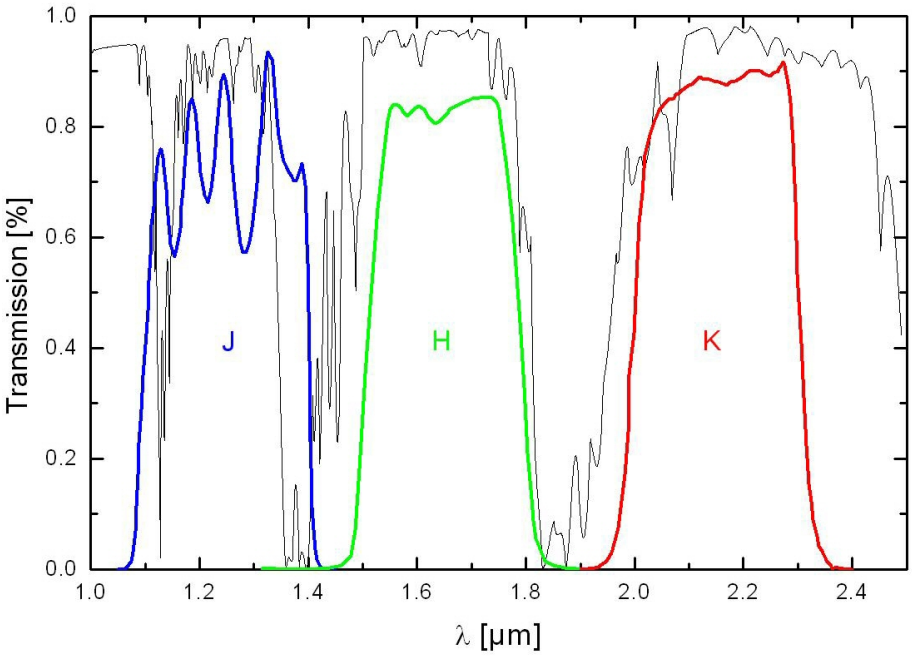


Figure 6: Transmission of the Earth's atmosphere in the near infrared. The transmission curves of the J-, H-, and K-band filters, which are adapted to the atmospheric transmission of the Earth's atmosphere, are shown in color.

## 1.4 Adaptive optics - ALFA and NAOS

The light from a star can be regarded as a plane-parallel wavefront, since the telescope aperture is negligible compared to the distance to the star. The light from the star is diffracted at the telescope aperture, creating a diffraction pattern in the image plane of the telescope that can be described by an Airy disk with a half-width:

$$\theta = 1.22 \frac{\lambda}{D}$$

If two objects are closer together than $\theta$, they are no longer resolved separately by the telescope. Thus, $\theta$ is referred to as the angular resolution of the telescope.

If a faint companion is located several multiples of $\theta$ away from the star, some starlight still reaches the position of the companion due to diffraction. The photon noise of this background signal makes it difficult to detect the companion. In order to successfully detect it next to the much brighter star, the interfering starlight must therefore be confined to an area around the star that is as small as possible. According to the law of diffraction, this can only be achieved with a large telescope aperture and observation at the shortest possible wavelength.

**Question:** Determine the angular resolution of an 8.2 m telescope in the K-band in milli-arcsec (mas).

Turbulence occurs in the Earth's atmosphere when the ground is heated by solar radiation, causing warm air masses (lower density) to rise and cold air masses (higher density) to sink. Since the refractive index of air depends on density, the speed of light varies in these air cells. In a simplified model, the Earth's atmosphere consists of air cells with a diameter of $r_0$ that move at a speed of $v_0 = 10\,\mathrm{m/s}$ at an altitude of 10 km.

The cell diameter $r_0$ is the Fried parameter and depends on the wavelength.

$r_0 \propto \lambda^{1.2}$

When a flat wavefront hits the atmosphere, it gets bent as it passes through the individual air cells. If you look at this distorted wavefront with a telescope, you get several diffraction-limited images of the star in the image plane. The number of these so-called speckles simply corresponds to the number of air cells that can be distributed across the telescope aperture:

$N_{Speckle} = (\frac{D}{r_0})^2$

The individual speckles overlap and thus produce a broad light distribution in the image plane, whose half-width is referred to as seeing:

$Seeing \propto \lambda^{-0.2}$

The individual air cells move across the telescope aperture over time, leading to a change in the speckle pattern within the time $\tau$:

$\tau = r_0/v_0$

**Question:** A star is observed with an 8.2 m telescope in the K-band. At $0.55\,\mu$m, the seeing during the observation is 1 arcsec ($r_0(0.55\,\mu\mathrm{m}) = 0.11\,\mathrm{m}$). Determine the seeing in the K-band and compare it with the angular resolution of the telescope. How many speckles make up the seeing-limited image of the star? At what frequency does the speckle pattern change?

While a close companion to a star might still be detectable in a diffraction-limited case, it can no longer be observed separately from the star in an image limited by seeing. In order to detect the companion, the atmospheric disturbances of the wavefront must be corrected. This correction is possible through the use of adaptive optics. The light collected by the telescope hits a deformable mirror and is reflected by it to the camera. With the help of a beam splitter, part of the light reaches a wavefront sensor, which determines the deformation of the wavefront. The surface of the deformable mirror is then adjusted using actuators on the back of the mirror so that the wavefront is parallelized during reflection. Since the wavefront and thus also the speckle image are only constant within the time $\tau$, the entire measurement and control process must take place within this time interval.

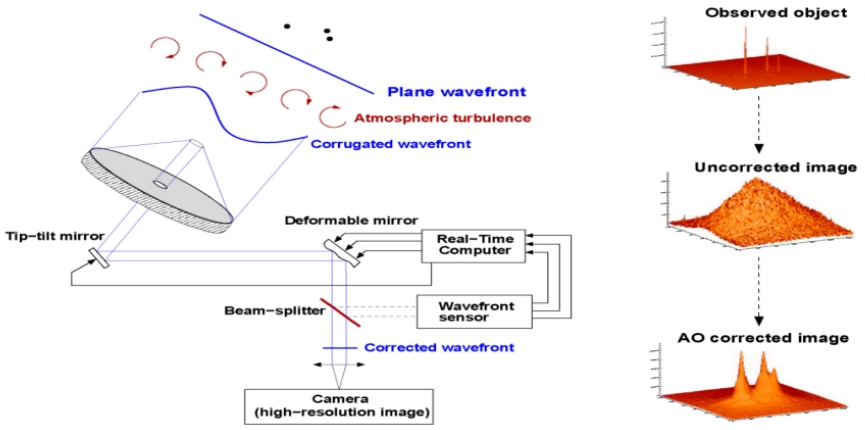


Figure 7: Functional principle of adaptive optics.

In this experiment, infrared data collected by the 3.5 m telescope at the Calar Alto Observatory (in Spain) and one of the four 8.2 m telescopes at the Paranal Observatory (in Chile) will be processed.

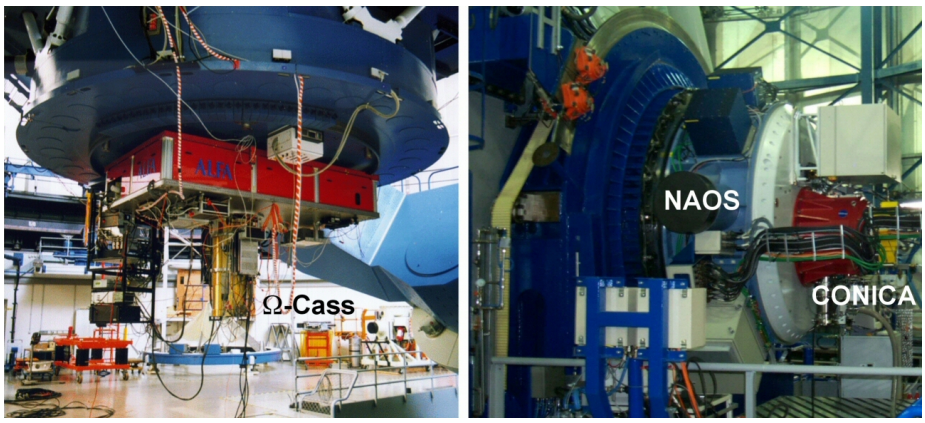


Figure 8: The image on the left shows the ALFA adaptive optics system (red) together with the infrared camera Ω-Cass in the Cassegrain focus of the 3.5 m telescope at the Calar Alto Observatory. The image on the right shows the Nasmyth focus of the 8.2 m telescope Yepun (UT4) at the Paranal Observatory. The NAOS adaptive optics system (light blue) is located in the beam path between the telescope and the infrared camera CONICA (red).

On the 3.5 m telescope at the Calar Alto Observatory the adaptive optics ALFA (Adaptive optics with a Laser For Astronomy) was used in combination with the infrared camera Ω-Cass, which was installed in the Cassegrain focus of the telescope (see Fig. 8). Ω-Cass works with a HgCdTe detector with 1024x1024 pixels and a pixel scale of $77.6 \pm 0.3$ mas/pixel. The operating temperature of the detector is 77 K. The adaptive optics system ALFA consists of a deformable mirror with 97 actuators, which is operated in conjunction with a

tip-tilt mirror[4]. The wavefront sensor is a Shack-Hartmann sensor that uses the visible component of starlight to analyze the wavefront.

The telescope Yepun (UT4) is one of four identical 8.2 m telescopes at the Paranal Observatory. The adaptive optics system NAOS (Nasmyth Adaptive Optics System) was installed at the Nasmyth focus of this telescope and was operated in conjunction with the infrared camera CONICA (Coudé Near Infrared Camera) (see Fig. 8). The detector in CONICA is a 1024x1024 InSb pixel array. The operating temperature of the detector is 35 K. CONICA has several optics with different field of views, e.g., the S13 ($13.23 \pm 0.05$ mas/pixel) or the S27 ($27.07 \pm 0.05$ mas/pixel) objective. Coronagraph masks can also be inserted into the image plane of the telescope. The adaptive optics system NAOS consists of a tip-tilt mirror that is operated in conjunction with a deformable mirror with 185 actuators. Two beam splitters allow either visible or infrared light to be used for analyzing the deformed wavefront. A Shack-Hartmann sensor is available for analyzing the wavefront in both spectral ranges.

## 1.5 The search for substellar companions of stars

As already described in Chapter 1, substellar objects (brown dwarfs and planets) cool down after their formation and become increasingly dim. Due to the low atmospheric temperatures, the maximum radiation of these objects is already in the near infrared. Today, adaptive optics can be used to image these faint objects as close companions of stars.

In most cases, many other objects can be seen in an image alongside the companion, but these are only coincidentally in the field of view and are in fact distant background stars. Since the companion is bound to the star, both objects move together in the same direction in the sky (orbital motion neglected).

Due to the movement of the star, its distance from the background objects changes over time. The distance between the star and its companion, on the other hand, remains constant, as both objects have the same proper motion. By comparing the distances of the detected objects from the star in two images, true companions of the star can be distinguished from background objects.

**Question:** The Sun moves at a speed of 250 km/s around the center of the Milky Way. Determine the apparent annual motion (in arcsec/yr) of our Sun for a stationary observer 10 light-years away. Determine the ratio of Jupiter's orbital motion to the Sun's proper motion.

The position of an object in the sky is most easily described in the geocentric equatorial coordinate system using the two coordinates right ascension ($\alpha$) and declination ($\delta$) (see Fig. 9 on the right). The reference plane is the celestial equator ($\delta = 0°$), which represents the projection of the Earth's equator onto the celestial sphere. The intersection of the Earth's orbital plane with the celestial sphere is the ecliptic, which is inclined by $\epsilon = 23.439°$ to the celestial equator. The Sun travels across the entire sky once a year on this orbit. The points of

[4]Tip-tilt mirror: A tiltable mirror that compensates for the movement of the center of light.

intersection between the ecliptic and the celestial equator are called the vernal equinox ($\alpha = 0°$, $\delta = 0°$) and the autumnal equinox ($\alpha = 180°$, $\delta = 0°$), respectively, because the Sun reaches these points at the beginning of spring and autumn. The movement of a star in the geocentric equatorial coordinate system is always the sum of the star's proper motion and its parallactic motion, which is caused by the Earth's rotation around the Sun.

The following applies to the star's proper motion during the time interval $\Delta t$:

$$\Delta RA = \mu_\alpha cos(\delta) \cdot \Delta t$$

$$\Delta Dec = \mu_\delta \cdot \Delta t$$

with $\mu_\alpha cos(\delta)$ and $\mu_\delta$ being the proper motions of the star in the right ascension and declination directions, respectively. The shift in the star's position caused by parallax depends on the equatorial coordinates of the star ($\alpha$, $\delta$) and the position of the Earth in its orbit. The parallax shift can be calculated using the inclination of the ecliptic to the celestial equator $\epsilon$, the geocentric ecliptic longitude of the Sun at the time of observation $\lambda_\odot$ and the parallax $\varpi$ of the star:

$$\Delta RA = \varpi(cos(\epsilon)sin(\lambda_\odot)cos(\alpha) - cos(\lambda_\odot)sin(\alpha))$$

$$\begin{aligned}\Delta Dec = \varpi(&sin(\epsilon)sin(\lambda_\odot)cos(\delta) - cos(\epsilon)sin(\lambda_\odot)sin(\alpha)sin(\delta) \\ &- cos(\lambda_\odot)cos(\alpha)sin(\delta))\end{aligned}$$

**Question:** Determine the geocentric ecliptic latitude of the Sun $\beta_\odot$.

**Question:** Consider a star that is at a distance $a$ from the Sun and, when viewed from Earth, is located exactly at the vernal equinox. Calculate the parallactic motion of the star in the geocentric equatorial coordinate system. Check your result in the geocentric ecliptic coordinate system using simple geometric considerations (see Fig. 9 on the left).

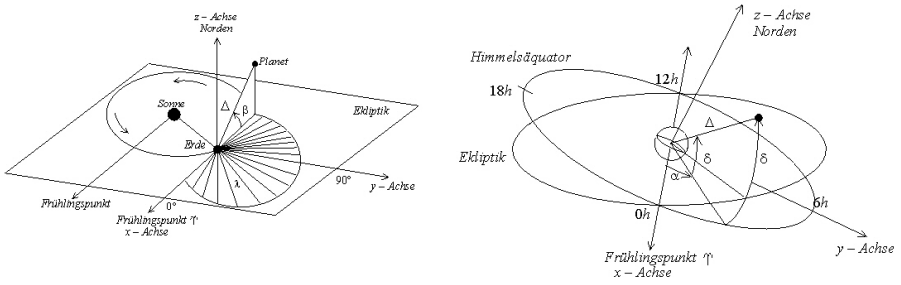


Figure 9: The geocentric-ecliptic (left) and geocentric-equatorial (right) coordinate systems.

# 2 Experiment procedure

## 2.1 Data Reduction

The reduction of raw data and the subsequent analysis of images is performed using the *MIDAS* (Munich Image Data Analysis System) program. *MIDAS* offers a wide range of different commands for image processing. In addition to these internal *MIDAS* commands, Shell commands can also be executed directly under *MIDAS*.

An overview of some important **Shell commands**:

| | |
|---|---|
| cd | returns to the home directory |
| cd name | changes to the directory name |
| inmidas | starts *MIDAS* |
| ls | displays the contents of the current directory |
| pwd | displays the path of the current directory |

An overview of some important ***MIDAS* commands**:

| | |
|---|---|
| average/image | averages multiple images |
| clear/chan o | clears all lines in the *MIDAS* display |
| comp | performs operations between images and variables |
| copy/display ? ? P | creates a Postscript copy of the *MIDAS* display |
| create/icataloge | creates an image catalog |
| load | loads an image |
| stat/image | outputs information about image statistics |
| @@ | executes a *MIDAS* program |

Commands are entered in *MIDAS* via the terminal. After entering a command, it can still be changed by moving the cursor to the appropriate position using the arrow keys (←→) and then making the desired changes. The command is then executed by pressing the enter key. All *MIDAS* commands that have already been entered can be retrieved in the command line using the arrow key (↑). This command can then be modified or executed directly.

Before you begin data reduction, first change from the base directory to the root directory of this experiment, irdata.

**cd irdata**

## 2.2 Jitter Technique

In the first part of the experiment, infrared images taken with the normal jitter technique will be reduced. The star GJ 702.1 was exposed in the K-band with the S13 objective from NAOS-CONICA.

Start *MIDAS* and use the command:

**ls**

to get an overview of the files and directories located in the directory *irdata*.

Now use the command:

**cd gj702**

to enter the *gj702* directory, where you will find all the data you need for the first part of the experiment. The directory contains 27 raw images of the star GJ 702.1 (prefix *bild*) and two flatfield images (prefix *flat*).

The first step is to generate the flatfield image. To do this, process the images *flat_on.bdf* and *flat_off.bdf*.

Load both images into the *MIDAS* display:

**load flat_on.bdf cent=512,512 scale=-2 cuts=f,sigma**
**load flat_off.bdf cent=512,512 scale=-2 cuts=f,sigma**

The parameters *cent*, *scale*, and *cuts* specify how the image should be displayed. *Cent* indicates the coordinates of the image center. *Scale* specifies the scaling factor with which the image is loaded. A negative value means a reduction by the specified factor. The displayed intensity values of the pixels are set with *cuts*=*x*,*y*, where *x* corresponds to the lowest (black) and *y* to the highest (white) pixel value displayed.

*flat_on.bdf* is the flatfield image and *flat_off.bdf* is the background image, which was taken with the same exposure time as the flatfield image. To remove the distracting background from the image, both images must be subtracted from each other:

**comp flat.bdf = flat_on.bdf - flat_off.bdf**

In order to correct for the different sensitivities of the pixels, the individual images must later be divided by the flatfield image. For this reason, the mean value of the pixel intensity in the flatfield image is normalized to 1.

This requires information about the image statistics, which can be obtained with the command:

**stat/image flat.bdf**

The field *mean* contains the mean value of the pixel values of the image *flat.bdf*. The flatfield image is normalized by simple division, where *mean* is the previously determined mean value of the flatfield image:

**comp flat.bdf = flat.bdf / mean**

Check whether the mean value of the flatfield image is now actually normalized to 1 by applying the command *stat/ima* to the image *flat.bdf* again. Now compare the reduced flatfield image with the raw image *flat_on.bdf*. To do this, load both images one after the other into the *MIDAS* display:

**load flat_on.bdf scale=-2 cuts=f,sigma**
**load flat.bdf scale=-2 cuts=f,sigma**

Describe (in the protocol) the most striking differences between the two images. How can these differences be explained?

In the next step, we will now turn our attention to the individual raw images of the star GJ 702.1. Load the individual images using the command:

**load bild1.bdf scale=-2 cuts=-5,100**
**load bild2.bdf scale=-2 cuts=-5,100**
**...**

You can also vary the *cuts* accordingly to display different pixel intensities in the *MIDAS* display.

Since the position of the telescope was slightly shifted from image to image (jitter technique), the star is always located at a different position on the detector. The bright background in the infrared can be removed from the images by simply subtracting two consecutive images from each other. All difference images are then divided by the flatfield image, which corrects for the different sensitivity of the individual pixels:

**comp s1.bdf = (bild1.bdf - bild2.bdf) / flat.bdf**
**...**
**comp s26.bdf = (bild26.bdf - bild27.bdf) / flat.bdf**

Compare the raw images (e.g., *image1.bdf*) with the reduced images (e.g., *s1.bdf*). Load the images alternately into the MIDAS display:

**load bild1.bdf scale=-2 cuts=-5,10**
**load s1.bdf scale=-2 cuts=-5,100**
**...**

Now save the raw image *image1.bdf* and the corresponding reduced image *s1.bdf* (for later display in the protocol) as a Postscript file (PS file for short). To do this, first load each image into the *MIDAS* display and copy the display to a PS file using the command:

**copy/display ? ? POSTSCRIPT**

This creates the PS file *screen00.ps*, which can then be renamed to for example *newname.ps* using the command:

**mv screen01.ps newname.ps**

Describe (in the protocol) the most striking differences between the two images. How can these differences be explained?

The next step is to shift the reduced individual images so that the telescope offset between the individual images is compensated for. The bright star GJ 702.1 can be used here as a reference object for measuring the image shift.

With the *MIDAS* program @@ *align ref pic*, the image *pic* can be moved so that it matches the reference image *ref*. Both images appear one after the other in the *MIDAS* display. Center the measurement box on the star with the mouse and confirm first with the left mouse button and then with the right mouse button:

**@@ align s1 s2**
**@@ align s1 s3**
**...**

The image suffix (*bdf*) is not written here!

The program first measures the positions of the star in both images and calculates the necessary shift in the x and y directions. The image *pic* is then shifted by the calculated value and saved as a new image with the suffix *_shifted*. Check whether the individual images have been shifted correctly. To do this, load the images into the *MIDAS* display, e.g.:

**load s2_shifted.bdf cent=512,512 scale=-2 cuts=-5,100**

Once the telescope offset has been corrected, the images can now be combined. To do this, first create an image catalog that contains all images:

**create/icatalog cat s1.bdf,*shifted.bdf**

When combining the individual images, either the mean value or the median can be calculated from the images:

**average/image average.bdf = cat.cat M ? average**
**average/image median.bdf = cat.cat M ? median**

Load the two results of the data reduction one after the other into the *MIDAS* display:

**load median.bdf scale=-3 cuts=-5,10**
**load average.bdf scale=-3 cuts=-5,10**

Now save the images *average.bdf* and *median.bdf* (for later display in the protocol) as PS files and discuss (in the protocol) the most striking differences between the two results of the data reduction. How can these differences be explained?

Now change the *cuts* in the image *median.bdf* so that faint objects are also displayed in the *MIDAS* display alongside the bright star. How many objects can you identify in the image?

Now determine the half-widths of the three brightest objects in the x and y directions in angular measure in milli-arcseconds (mas). Compare the measured half-widths with the angular resolution of the telescope.

To do this, first load the image into the *MIDAS* display and then use the *MIDAS* command:

**center/gauss**

A measurement box appears in the *MIDAS* display, which you can move over the image with the mouse. You can change the size of the box using the arrow keys (←→↑↓). Move the box over an object in the image and change the box size so that only the object is inside the box. Activate the measurement process by pressing the left mouse button. After the measurement data has been output to the terminal, you can now measure another object. To end the measurement process, press the right mouse button. The position of each object is specified in the fields (*xcenter*, *ycenter*) with the measurement errors (*xerr*, *yerr*). The half-widths in the x and y directions can be found in the fields (*xfwhm*, *yfwhm*). These are specified in pixels and can be converted to angles using the pixel scale of the CONICA S13 objective.

## 2.3 Extended Jitter Technique

In this part of the experiment, infrared data recorded using the extended jitter technique will be reduced. The star HD 175742 was observed with NAOS-CONICA in the K-band using its S27 objective. In addition, a coronagraph mask was inserted into the image plane of the telescope, which attenuates the light of the star by a factor of 10000 (semitransparent coronagraph with 4 masks). The raw data can be found in the *hd175* directory. The object images are labelled with the prefix (*bild*), and the corresponding background images with the prefix (*back*). First, create the flatfield image from the raw image *flat_on.bdf* and the corresponding background image *flat_off.bdf* and normalize it to 1.

Since the coronagraph masks are located at fixed positions in the image plane, the jitter technique cannot be applied. Therefore, the extended jitter technique is used, in which the object and the sky background are observed alternately. The background images are subtracted from the object images and divided by the flatfield image again. Since the position of the star behind the coronagraph mask varies slightly from image to image, the difference images (prefix *s*) must also be shifted relative to each other. To do this, use the *MIDAS* program *aligncoro*:

**@@ aligncoro s1 s2**
**@@ aligncoro s1 s3**
**...**

Note: The image suffix (*bdf*) is not used here!

The image *s1.bdf* is again the reference image on which all other images are centered. You can use the star HD 175742, which is behind the coronagraph mask, as a reference object. Select a box size that is just large enough to fit the star disk. The size of the measurement box can be adjusted using the arrow keys.

Once you have shifted all images relative to the first image, the individual images can be combined. Create the median of all individual images and load the image into the *MIDAS* display:

**load median.bdf scale=-2 cuts=0,100**

How many objects are detected next to the bright star HD 175742?

Vary the *cuts* so that as many of the detected objects as possible are visible on the display, and save the image (for later display in the protocol) as a PS file.

Determine the position of all objects and calculate their separations from the star HD 175742 in pixel coordinates. Calculate the separations in the x and y directions as well as the total separation. Use the pixel scale of the CONICA S27 objective to convert these separations into angular separations (in mas) (don't forget to calculate also the error!).

CONICA is oriented so that the axes of the detector coincide with the coordinate axes of the geocentric equatorial coordinate system. The right ascension increases to the left and the declination increases upwards (left-handed coordinate system).

## 2.4 Data analysis

Two years before the NAOS-CONICA observations the star HD 175742 was already imaged with ALFA and Ω-Cass on the 3.5 m telescope at the Calar Alto Observatory. You can find this image in the *alfa* directory. Change to this directory:

**cd ..**
**cd alfa**

and load the ALFA image of the star:

**load hd175.bdf scale=-2 cuts=-200,4000**

Search the ALFA image for the objects you previously identified in the NAOS-CONICA image near the star. Vary the *Cuts* accordingly so that the objects are clearly visible, and save the image as a PS file (for later display in the protocol). Note the different pixel scales of the detectors used. The ALFA image is also rotated by approximately 22 ° compared to the NAOS-CONICA image.

Again, determine the angular separation of the detected objects from the star HD 175742 (don't forget to calculate the error!).

Now compare the angular separations from the ALFA image with the angular separations, measured in the NAOS-CONICA image, and conclude whether the detected objects are companions of the star or background stars. Note the astrometry of the star HD 175742:

$\alpha = 18\text{h } 55\text{m } 53\text{s}$, $\delta = 23^\circ\ 33'\ 24''$
$\mu_\alpha cos(\delta) = 130.79\,\text{mas/yr}$, $\mu_\delta = -283.07\,\text{mas/yr}$
$\varpi = 46.64\,\text{mas}$

Calculate the expected movement of the star HD 175742 between the ALFA and NAOS-CONICA observations. The time difference between the two images is $\Delta t = 826$ days. The geocentric ecliptic longitude of the Sun was $\lambda_\odot = 34.8105^\circ$ during the ALFA observation and $\lambda_\odot = 128.9553^\circ$ during the NAOS-CONICA observation.

The angular separation of the objects in the ALFA image can be calculated using the motion of the star HD 175742 and the measured angular separations of the objects in the NAOS-CONICA image. To do this, assume that only the star has a measurable proper motion, while all other objects are fixed background stars. Compare the calculated angular separations with the measured angular separations in the ALFA image.